



ANALYSIS OF PERIODICALLY VARYING GEAR MESH SYSTEMS WITH COULOMB FRICTION USING FLOQUET THEORY

M. VAISHYA AND R. SINGH

*Acoustics and Dynamics Laboratory, Department of Mechanical Engineering,
The Ohio State University, Columbus, OH 43210-1107, U.S.A. E-mail: singh.3@osu.edu*

(Received 14 April 2000, and in final form 2 November 2000)

This article presents a new analytical model of a gear pair with time varying mesh stiffness, viscous damping and sliding friction parameters. Unlike previous models, the excitation consists of three separate terms, namely the unloaded transmission error, time-invariant external torque and the periodically varying sliding friction force. A Coulomb friction model is considered using first a quasi-static mean transmitted load that is represented by the Meissner equation. Then, a truly dynamic force between gear teeth is described that leads to a triangular function, and after appropriate substitutions, this assumes the form of the Bessel equation of the one-third order. For the damped Meissner equation, the forced vibration response is found with the application of Floquet theory. Exact integrals are calculated for the state transition matrix in a piecewise manner, instead of using the Fourier series expansion, thus eliminating the mode truncation errors. From the state transition matrix, unstable zones are identified and the actual forced response of the system is found in terms of dynamic transmission error for these zones. With the aid of an example, the significance of sliding friction on system response and stability is examined. Finally, key advantages and the need for analytical methods are demonstrated for such systems.

© 2001 Academic Press

1. INTRODUCTION

The physical mechanism of gear meshing demonstrates a wide spectrum of dynamic characteristics, including significant time-varying mesh stiffness and damping changes during one tooth meshing cycle. Additionally, the instantaneous number of teeth in contact, governs the load distribution and sliding resistance acting on the individual teeth. Consequently, the geared system responds to a combined excitation of transmission error due to profile deviations, periodic variations in system parameters and periodically varying sliding friction. Such complexities have led prior researchers [1–14] to adopt numerical approaches or approximate analyses, with many simplifying assumptions. For example, many researchers have developed the dynamic models of gears [1] by neglecting friction or assuming constant mesh parameters. Although sliding force amplitudes are small compared to the mean transmitted loads, the large oscillatory component of friction force is potentially a major excitation source [2]. Iida *et al.* [3] estimated the response in terms of shaft deflections in the friction direction. Borner and Houser [2] extended this formulation to helical gears, based on the instantaneous load distribution that is computed from boundary-element-type contact analysis. The effect of friction on torsional dynamics was studied by Radzimovsky and Mirarefi [4] for a four-square test rig.

It is well known that the contact characteristics of gear teeth dictate the spatial variations in meshing stiffness and viscous damping parameters [5–7]. Iwatsubo *et al.* [8] investigated the coupling between lateral and torsional vibrations using a six-degree-of-freedom model with time-varying mesh properties. Kahraman and Singh [9] studied the interactions between variable mesh stiffness and clearance non-linearities for single- and three-degree-of-freedom systems using digital simulation techniques. Conversely, semi-analytical methods were applied by Padmanabhan and Singh [6] to analyze the non-linearities for the gear systems. Oh *et al.* [10] considered both time and angular domain formulation using the Lagrangian principle and showed that the ensuing non-linear dynamic response was consistent with the energy conservation principle. However, in all of these studies, friction between gear teeth and its cyclic nature were either ignored or incorporated as an equivalent viscous damping term [11]. Recently, Hochmann [12] has studied the effect of periodic friction on torsional dynamics using a Fourier series expansion, with the assumption of constant mesh stiffness and damping. In the literature, no reference could however be found for a full analytical model of a gear pair, that includes interactions among time-varying system parameters, sliding friction and transmission error excitation.

Due to large fluctuations in mesh compliance, stability emerges as an important criterion in gear systems. Some stability characteristics of gear systems were studied by Iwatsubo *et al.* [8] and Kumar *et al.* [13] using state-space methods. In an earlier work, Benton and Seireg [14] showed the differences in superharmonic response arising due to rectangular and sinusoidal mesh stiffness variations. Blankenship and Singh [11] analyzed the parametric resonances in mechanical oscillators as introduced by factors like stiffness variations and angular modulation effects, from the standpoint of understanding side-band phenomenon. Overall, none of these studies specifically considered sliding resistance in the system, and hence the influence of friction on dynamic characteristics remains ill-understood.

In this article, a new analytical model will be developed that incorporates sliding resistance in the dynamic equations for a spur gear pair. By defining all the parameters in a piecewise manner, the system is translated into a linear time-varying (LTV) form. With the application of Floquet theory, both homogenous and forced responses will be derived for a combined excitation of static transmission error, parametric variation of mesh stiffness and periodic frictional torque. Analytical solutions are then sought to study the influence of friction on the dynamic behavior of gears. The stability characteristics of gears will be investigated using the concept of state transition matrix. An example is chosen to illustrate some of the concepts.

2. PROBLEM FORMULATION

2.1. REPRESENTATION OF GEAR EXCITATIONS

The generic gear pair is modelled as a purely torsional vibration system (Figure 1). Mesh stiffness $k(t)$ is a result of Hertzian deformation as well as the cantilever bending of the teeth. Non-conjugacy of the tooth profiles manifests as a displacement excitation at the mesh, commonly referred to as the unloaded static transmission error, $\varepsilon(t)$. Sliding on the gear tooth surface causes a frictional force F_f along the off-line of action direction, which is designated as the η -axis. As the gears roll, the tooth interface point moves along the contact line or the line of action (ξ direction). This linearly varying value of $\xi_p(t)$ and $\xi_g(t)$ result in a time-varying torque T_f about the two gear axes, which will also depend upon the coefficient of friction (μ) and the normal load. Additionally, external torques T_p and T_g act on the pinion and the gear respectively. The gears rotate with mean angular speeds of

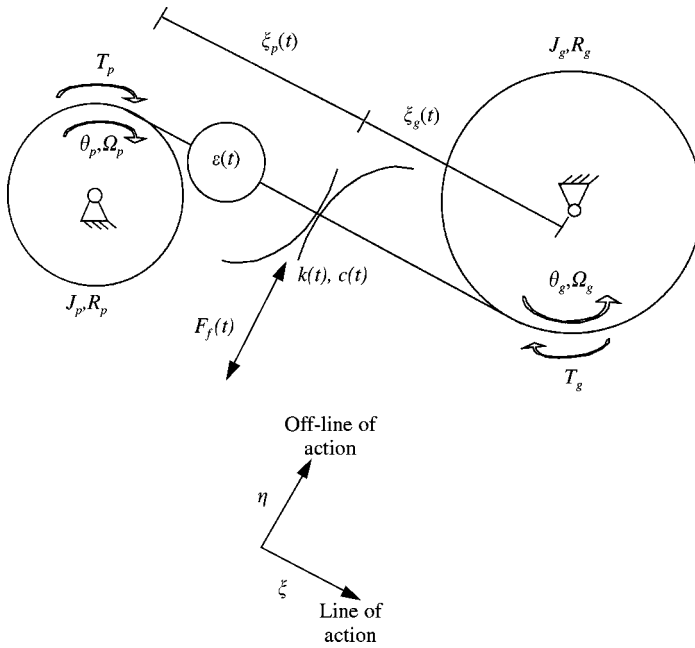


Figure 1. Dynamic model of a gear pair with sliding friction.

Ω_p and Ω_g , whereas θ_p and θ_g represent the vibratory angular displacements from the mean position.

2.2. PARAMETRIC VARIATIONS WITHIN ONE MESH PERIOD

For most practical designs of spur gears, the profile contact ratio Γ varies between 1.0 and 2.0. This implies that two teeth are in contact for $(\Gamma - 1)$ fraction of the total time, and a single tooth is transmitting the torque during the rest of the mesh cycle. In Figure 2, the beginning of the mesh cycle at $t = 0$ is defined to be coincident with the initiation of contact for the second tooth. As the gears roll, the first tooth leaves contact and there is a step reduction in the meshing stiffness $k(t)$ of the system. The load is assumed to be distributed equally amongst all the teeth in contact, hence its value will be doubled for the second tooth. Till this instant t_a , the sliding velocity V_s on the two pairs of teeth is opposite in direction, and consequently, so is the friction force F_f . The second critical point occurs at t_b when the zone of contact passes through the pitch point, and the direction of the sliding velocity for tooth 2 reverses [Figure 2(c)]. Finally, the third gear tooth comes into engagement at t_c and this constitutes one gear mesh cycle. Simplified variation of system parameters and the major excitations are sketched in Figure 2. These parameters can be represented in a mathematical form by equations (1-6).

(1) Load distribution $N(t)$ of Figure 2:

$$\begin{aligned} N_1(t) = N_2(t) = N/2, & \quad 0 \leq t < t_a, \\ N_1(t) = 0; N_2(t) = N, & \quad t_a \leq t < t_c, \end{aligned} \tag{1a-c}$$

here, $N = T_p/R_p$.

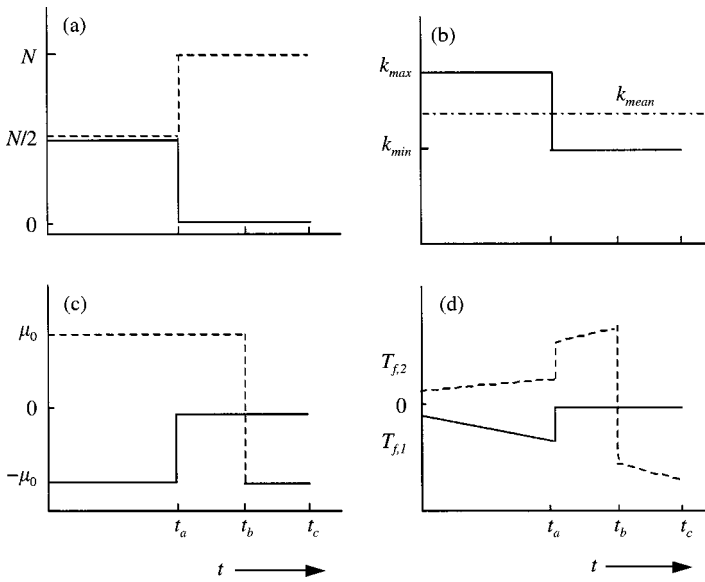


Figure 2. Simplified periodic variations as functions of gear mesh position. Key: —, first tooth; ---, second tooth. (a) Load distribution function $N(t)$; (b) mesh stiffness $k(t)$; (c) coefficient of friction μ ; (d) friction torque T_f .

(2) Mesh stiffness $k(t)$ of Figure 2:

$$k(t) = k_{mean}(1 + \beta(t)),$$

where

$$\beta(t) = (k_{max}/k_{min} - 1), \quad 0 \leq t < t_a, \tag{2a-c}$$

$$\beta(t) = (k_{min}/k_{max} - 1), \quad t_a \leq t < t_c.$$

The time-averaged mean stiffness k_{mean} is given by

$$k_{mean} = \langle k(t) \rangle_t = \frac{1}{t_c} \int_0^{t_c} k(t) dt = k_{max}(\Gamma - 1) + k_{min}(-\Gamma + 2). \tag{3}$$

(3) Coefficient of friction μ of Figure 2:

$$\mu_1 = +\mu_0 \operatorname{sgn}(t - t_a) \quad \text{for } 0 \leq t < t_a. \tag{4a, b}$$

$$\mu_2 = -\mu_0 \operatorname{sgn}(t - t_b) \quad \text{for } \forall t,$$

In equation (4), μ_0 is the coefficient of friction of the gear surface material.

(4) Frictional torque T_f of Figure 2:

$$\begin{aligned} T_{f,1} &= \gamma_{11} + \beta_{11}t \quad \text{and} \quad T_{f,2} = \gamma_{21} + \beta_{21}t, & 0 \leq t < t_a, \\ T_{f,1} &= \gamma_{12} + \beta_{12}t \quad \text{and} \quad T_{f,2} = \gamma_{22} + \beta_{22}t, & t_a \leq t < t_b, \\ T_{f,1} &= \gamma_{13} + \beta_{13}t \quad \text{and} \quad T_{f,2} = \gamma_{23} + \beta_{23}t, & t_b \leq t < t_c, \end{aligned} \tag{5a-c}$$

where parameters γ and β are specific to the gear pair design and depend on the tribological conditions and meshing kinematics.

(5) Sliding velocity V_s :

$$V_{s,i} = \alpha_{p,i} R_p \Omega_p - \alpha_{g,i} R_g \Omega_g. \quad (6)$$

In equation (6), α represents the gear roll angle, which is defined between the tangent to tooth profile at the point of contact and a radial line to the imaginary point when the tooth and base circle intersect. Due to the involute form of profile, α varies linearly with time for a constant angular speed Ω . From this, the sliding velocity is found as the difference between the surface tangential velocities at the point of contact for each tooth in mesh.

2.3. OBJECTIVES AND SCOPE

The main objectives of this paper are to (1) develop an analytical model for the system in Figure 1 that incorporates periodic sliding resistance due to friction, (2) apply Floquet theory to determine closed form solutions for a combined excitation of static transmission error, parametric variation of mesh stiffness and frictional torque, (3) investigate the influence of friction and other time-varying parameters (Figure 2) on the torsional dynamics of a spur gear pair, and (4) study the stability characteristics of the system with reference to relevant design parameters.

Essential steps of our methodology are as follows. All the system parameters and excitations are first defined in three piecewise continuous regimes within a tooth mesh cycle, as shown in Figure 2, and the corresponding equations of motion are written for an LTV system. Second, the Coulomb friction is considered to act on a quasi-static mean transmitted load, such that friction only acts as an external excitation. This system can be represented in the form of a damped Meissner equation. Third, Floquet theory is applied to find analytical solutions for both homogenous and forced vibration response in terms of dynamic transmission error, for a combined excitation of static transmission error, parametric variation of mesh stiffness and frictional torque. Fourth, the Coulomb friction model is applied on the dynamic mesh load between gear teeth, which results in triangular coefficients in the equation of motion. With appropriate substitutions, this is reduced to the form of a Bessel equation of the one-third order. Since closed form expressions for integrals of Bessel function do not exist, a semi-analytical approach is applied for predicting the response for this case. Fifth, for both the cases, the state transition matrix is computed and from its eigenvalues, dynamic stability conditions are studied. Finally, using the example of a practical gear pair, the influence of friction and other parameters on dynamic behavior and stability is examined.

In our formulation, several assumptions have been made for the purpose of clarity. The gear pair is represented by a single-degree-of-freedom torsional system, while flexural vibrations and their coupling with torsional motion are ignored. Subsequent analysis however shows that the solutions can be easily extended to higher degree systems in a future study. Both mesh stiffness and damping are assumed to follow a rectangular waveform, entailing a step change at the tooth transition points. Sliding velocity at the gear and pinion teeth surface, which is required to find the direction of friction force, is determined only from gear mesh kinematics. Hence it does not accommodate the instantaneous angular velocity changes due to the vibratory motion. Furthermore, no distinction is made between spatial and temporal variations of parameters and all parameters are therefore assumed to be functions of time only. These two assumptions allow for the whole study to be carried out as an LTV analysis explicitly in the time domain.

3. ANALYTICAL MODEL WITH SLIDING FRICTION

3.1. GOVERNING EQUATIONS

For the dynamic system of Figure 1, the equations of torsional motion can be written for the pinion and the gear (subscripts p and g respectively). Refer to Appendix A and Figure 1 for the identification of symbols.

$$\begin{aligned} J_p \ddot{\theta}_p + c(t)(\dot{\theta}_p R_p - \dot{\theta}_g R_g - \dot{\varepsilon})R_p + k(t)(\theta_p(t)R_p - \theta_g(t)R_g - \varepsilon(t))R_p \\ = T_p + \sum_i \mu_i(t)N_i(t)\zeta_{pi}(t), \end{aligned} \quad (7)$$

$$\begin{aligned} J_g \ddot{\theta}_g + c(t)(\dot{\theta}_g R_g - \dot{\theta}_p R_p + \dot{\varepsilon})R_g + k(t)(\theta_g(t)R_g - \theta_p(t)R_p + \varepsilon(t))R_g \\ = -T_g - \sum_j \mu_j(t)N_j(t)\zeta_{gj}(t). \end{aligned} \quad (8)$$

Here i, j are the indices of the particular teeth in contact. Recognizing that this is a semi-definite system, define the dynamic transmission error (DTE) as $\delta(t) = R_p\theta_p(t) - R_g\theta_g(t)$, such that equations (7 and 8) reduce to a single equation:

$$\begin{aligned} J_p J_g \ddot{\delta} + c(t)(\dot{\delta} - \dot{\varepsilon})(R_p^2 J_g + R_g^2 J_p) + k(t)(\delta(t) - \varepsilon(t))(R_p^2 J_g + R_g^2 J_p) \\ = (T_p R_p J_g + T_g R_g J_p) + J_g R_p \sum_i \mu_i(t)N_i(t)\zeta_{pi}(t) + J_p R_g \sum_j \mu_j(t)N_j(t)\zeta_{gj}(t). \end{aligned} \quad (9)$$

3.2. ALTERNATE FRICTION FORMULATIONS

In our study, two kinds of variations in sliding forces are considered. Formulation A is based on the quasi-static, time-averaged transmitted torque and formulation B is based on the dynamic mesh forces. Thus, the expressions for friction force for the two cases can be written as follows:

$$\text{Formulation A: } F_f(t) = \mu_i N(t). \quad (10)$$

$$\text{Formulation B: } F_f(t) = \mu_i(k(t)\delta(t) + c(t)\dot{\delta}(t)). \quad (11)$$

In addition, there are two other significant excitations, the mean load that may influence the parametric excitation and a displacement function due to profile variations on the tooth surface, the latter often known as the unloaded static transmission error $\varepsilon(t)$. An inspection of the $\varepsilon(t)$ curves shows that these are best expressed by a Fourier series expansion, where typically up to eight harmonics of meshing frequency provide an adequate representation. In this manner, the gear dynamics problem is defined in three distinct piecewise linear regions as shown in Figure 2. Relevant equations of motion for formulation A are given as follows, where α_m is the total roll angle spanned in one mesh cycle:

$$\begin{aligned} J_e \ddot{\delta} + J_i(c_a \dot{\delta} + k_a \delta(t)) = T_e + J_i(c_a \dot{\varepsilon} + k_a \varepsilon(t)) \\ - \mu_0 N \alpha_m R_p (J_p R_g - J_g R_p) / 2, \quad 0 \leq t < t_a, \end{aligned} \quad (12)$$

$$\begin{aligned} J_e \ddot{\delta} + J_i(c_b \dot{\delta} + k_b \delta(t)) = T_e + J_i(c_b \dot{\varepsilon} + k_b \varepsilon(t)) \\ + \mu_0 N (R_p J_g \zeta_{p2}(t) + R_g J_p \zeta_{p1}(t)), \quad t_a \leq t < t_b, \end{aligned} \quad (13)$$

$$J_e \ddot{\delta} + J_t(c_b \dot{\delta} + k_b \delta(t)) = T_e + J_t(c_b \dot{\varepsilon} + k_b \varepsilon(t)) - \mu_0 N(R_p J_g \zeta_{p2}(t) + R_g J_p \zeta_{p1}(t)), \quad t_b \leq t < t_c. \quad (14)$$

In these equations, the following equivalent symbols have been used:

$$J_e = J_p J_g, \quad J_t = J_p R_g^2 + J_g R_p^2, \quad T_e = J_p R_g T_g + J_g R_p T_p. \quad (15a-c)$$

Equations (12–14) may be represented in a general form as follows, where m_e , c_e and k_e are equivalent dynamic parameters:

$$m_e \ddot{\delta} + c_e \dot{\delta} + k_e \delta(t) = \sum F_e(t). \quad (16)$$

Similarly for formulation B, we get

$$J_e \ddot{\delta} + (J_t + \mu_0 \alpha_m R_p J_d/2)(c_a \dot{\delta} + k_a \delta(t)) = T_e + (J_t + \mu_0 \alpha_m R_p (J_p R_g - J_g R_p)/2)(c_a \dot{\varepsilon} + k_a \varepsilon(t)), \quad (17)$$

$$J_e \ddot{\delta} + (J_t - \mu_0 R_p J_g \zeta_{p2}(t) - \mu_0 R_g J_p \zeta_{p1}(t))(c_b \dot{\delta} + k_b \delta(t)) = T_e + (J_t - \mu_0 R_p J_g \zeta_{p2}(t) - \mu_0 R_g J_p \zeta_{p1}(t))(c_b \dot{\varepsilon} + k_b \varepsilon(t)), \quad (18)$$

$$J_e \ddot{\delta} + (J_t + \mu_0 R_p J_g \zeta_{p2}(t) + \mu_0 R_g J_p \zeta_{p1}(t))(c_b \dot{\delta} + k_b \delta(t)) = T_e + (J_t + \mu_0 R_p J_g \zeta_{p2}(t) + \mu_0 R_g J_p \zeta_{p1}(t))(c_b \dot{\varepsilon} + k_b \varepsilon(t)). \quad (19)$$

Equation (17) can be written in a similar manner as equation (16). Conversely, for equations (18) and (19), the friction moment arm $\zeta_{pi}(t)$ is linearly changing with time, as shown in equation (20a, b). Here, α_0 is the roll angle at the start of the mesh cycle, referred to as the highest point of single tooth contact.

$$\zeta_{p1}(t) = (\Omega_p t + \alpha_m + \alpha_0) R_p, \quad \zeta_{p2}(t) = (\Omega_p t + \alpha_0) R_p. \quad (20a, b)$$

Consequently, the general formulation for equations (18 and 19) is

$$m_e \ddot{\delta} + c_e(1 + \beta_c t) \dot{\delta} + k_e(1 + \beta_k t) \delta(t) = \sum F_e(t). \quad (21)$$

It may be noted that the homogenous part of equation (16) is independent of friction, thus effectively reducing the problem into a general second order equation, where sliding friction only acts as an external excitation. On the other hand, friction terms appear on the left-hand side of equation (21). Consequently, μ becomes a system parameter and it would then lead to dynamic interactions between the sliding characteristics and the periodic system parameters.

4. STATE TRANSITION MATRIX AND FLOQUET THEORY

4.1. STATE TRANSITION MATRIX REPRESENTATION

The above two sets of equations (12–14) and (17–19) can be represented in the state space form as follows. In equation (22), \mathbf{x} and \mathbf{f} are the generalized state vectors for displacement and force, respectively, whereas \mathbf{G} is the system matrix:

$$\dot{\mathbf{x}}(t) = \mathbf{G}(t)\mathbf{x}(t) + \mathbf{f}(t), \quad (22)$$

where

$$\begin{aligned} \mathbf{G}(t) &= \mathbf{G}_1(t), & 0 \leq t < t_a, \\ \mathbf{G}(t) &= \mathbf{G}_2(t), & t_a \leq t < t_b, \\ \mathbf{G}(t) &= \mathbf{G}_3(t), & t_b \leq t < t_c, \end{aligned} \quad (23a-c)$$

and

$$\mathbf{x}(t) = \begin{Bmatrix} \delta(t) \\ \dot{\delta}(t) \end{Bmatrix}. \quad (24)$$

The solution over one complete mesh cycle t_c is written in the form of a state transition matrix (Φ). For a piecewise periodic system, this matrix may further be decomposed into Φ over smaller segments [15], where the functions are continuously differentiable and analytical solutions to the homogenous equation exist. Thus,

$$\Phi_m = \Phi(t_c, 0) = \Phi(t_c, t_b) \Phi(t_b, t_a) \Phi(t_a, 0), \quad 0 \leq t < t_c. \quad (25)$$

Each of the individual $\Phi(t_1, t_2)$ is evaluated from the Wronskian matrix (\mathbf{W}), whose columns are constituted by the eigenvectors of the governing equation in the corresponding interval:

$$\Phi(t_1, t_2) = \mathbf{W}(t_2) \mathbf{W}^{-1}(t_1), \quad t_1 \leq t < t_2. \quad (26)$$

Using the periodic property of the state transition matrix, Floquet theory extends this to states of the system that are apart by more than one full period [16]. Thus, the state transition matrix over n cycles is given by

$$\Phi(nt_c, 0) = \Phi(t_c, 0)^n. \quad (27)$$

Equation (27) is extremely useful on two accounts. First, it drastically reduces the computation and secondly, it allows easy computation of the inverse of the matrix, thus making analytical solutions possible.

4.2. CALCULATION OF Φ FOR FORMULATION A

When dynamic load variations are not considered in the evaluation of friction, the problem takes the form of a damped Meissner's equation [15]. Both stiffness and damping follow a rectangular waveform. Each subinterval is characterized by constant coefficients and hence the results of a classical second order system can be directly applied. Although there are only two such sub-intervals, this analysis considers three segments, for the sake of generality when the forcing function is included. For each of the equations (12-14), the Wronskian matrix is given by equation (28), where λ_i s are the eigenvalues of the second order equation

$$\mathbf{W}_{1,2,3}(t) = \begin{bmatrix} e^{\lambda_1 t} & e^{\lambda_2 t} \\ \lambda_1 e^{\lambda_1 t} & \lambda_2 e^{\lambda_2 t} \end{bmatrix}. \quad (28)$$

4.3. CALCULATION OF Φ FOR FORMULATION B

Since equation (17) has constant coefficients for $0 \leq t < t_a$, the Wronskian and transition matrices are similar to equation (28). However, in equations (18) and (19), both stiffness and damping coefficients take the sawtooth form, due to the time varying moment arm. Since no analytical solutions exist for this problem, numerical methods must be applied. However, by ignoring the damping term and with appropriate substitution of variables, the equations converge to the form of Stokes equation [15]. Now the corresponding behavior of the system may be analytically studied. Using the linear relationship from equation (20a, b), the corresponding homogenous equation may be written as

$$\ddot{\delta} + (\beta_1 t + \beta_2)\dot{\delta}(t) = F(t), \quad t_a \leq t < t_b,$$

where

$$\begin{aligned} \beta_1 &= -\mu_0 R_p J_d \Omega_p k_b / J_e, \\ \beta_2 &= \left(\begin{array}{l} J_t - \mu_0 R_p J_d \alpha_a - \mu R_g J_p (R_p + R_g) \tan \varphi \\ -\mu_0 R_p (J_p R_g - J_g R_p) \Omega_p t_a \end{array} \right) \frac{k_b}{J_e}. \end{aligned} \tag{29a-c}$$

In equation (29), φ is the transverse pressure angle of the gears. A similar expression can be found for $t > t_b$. For a sawtooth coefficient, one possible solution is given by a pair of Bessel functions of order 1/3 and $-1/3$. Thus, the Wronskian can be computed, where J represents the Bessel function [15]

$$\mathbf{W}(t) = \begin{bmatrix} \sqrt{\beta_1 t + \beta_2} J_{1/3}(\sigma) & \sqrt{\beta_1 t + \beta_2} J_{-1/3}(\sigma) \\ (\beta_1 t + \beta_2) J_{-2/3}(\sigma) & -(\beta_1 t + \beta_2) J_{2/3}(\sigma) \end{bmatrix}, \quad \sigma = 2(\beta_1 t + \beta_2)^{2/3} / (3\beta_1). \tag{30a, b}$$

With the knowledge of the Wronskian for all individual time intervals, the state transition matrix for one complete mesh period is calculated:

$$\Phi = \mathbf{W}_3(t_c) \mathbf{W}_3^{-1}(t_b) \mathbf{W}_2(t_b) \mathbf{W}_2^{-1}(t_a) \mathbf{W}_1(t_a) \mathbf{W}_1^{-1}(0). \tag{31}$$

5. FORCED RESPONSE OF A GEARED SYSTEM

5.1. SPUR GEAR PAIR EXAMPLE

In order to illustrate some of the concepts presented in this paper, a case study is carried out using a non-unity ratio spur gear pair. Important parameters for this example are given in Table 1. It may be noted that the variation in stiffness is very significant (over $\pm 30\%$), thus lending itself to a potential stability problem. Table 1 also shows the calculated time instant values at the three critical points, at an input speed of 1500 rpm. The profile contact ratio Γ of the gear mesh can be varied by altering the outside diameter of the two gears. This results in shifting of points t_a and t_b , thus changing the periods of parameter variations. Subsequently, all these parameters are substituted in equations (28–31) to obtain the state transition matrix for the system and its eigenvalues, for the two cases considered previously. The critical time instants of a mesh cycle are related to other parameters of Table 1 as follows, where Π_p is the number of teeth in the pinion:

$$\frac{t_a}{t_c} = \Gamma - 1, \quad t_c = \frac{60}{\Omega_p} \times \frac{1}{\Pi_p}. \tag{32, 33}$$

TABLE 1

Gear design parameters and critical time instant values for one mesh cycle

Number of teeth Π_p, Π_g	25, 31
Center distance	88.9 mm
Profile contact ratio Γ	1.433
Input speed Ω_p	1500 rpm
Input torque T_p	226 N m
k_{mean} (N/m)	5.68×10^8
k_{max} (N/m)	7.20×10^8
k_{max}/k_{min}	1.667
Lowest point of single tooth contact (t_a)	0.693 ms
Pitch point (t_b)	1.148 ms
Highest point of single tooth contact (t_c)	1.600 ms

5.2. CLOSED-FORM SOLUTION

For a LTV system, the state transition matrix can be applied to compute the response under a periodic excitation. The tractability of the solution depends both on the excitation characteristics and the nature of the state transition matrix. In general, the problem is overcome by expanding the forcing function as well as the time-varying parameters as Fourier coefficients. Clearly, this will lead to errors due to truncation of modes and also increase the computations significantly. However, it should be noted that as the number of piecewise linear segments within a mesh cycle increases, such as in the case of a more realistic stiffness profile, analytical solutions could become computationally quite extensive. In the following sections, the corresponding integrals are found analytically for all possible excitation time histories for the geared system, comprising of sinusoids, ramps and constant loads. Unfortunately, this could not be extended to sawtooth coefficients because the homogenous solution in the form of Bessel functions is not integrable in a closed form.

A forced response of the system can be found using the Cauchy formulation [17], where $F(t)$ is an arbitrary forcing function:

$$x(t) = \mathbf{W}(t)\mathbf{W}^{-1}(0)\mathbf{x}(0) + \int_0^t \mathbf{W}(t)\mathbf{W}^{-1}(\tau) \mathbf{f}(\tau) d\tau, \quad \mathbf{f}(t) = \left\{ \begin{matrix} 0 \\ F(t) \end{matrix} \right\}. \quad (34, 35)$$

Ignoring the initial state of the system, the properties of the transition matrix may be used for deriving the value of the total response of the system. Using $\Phi(t, 0) = \Phi(t, \tau) \Phi(\tau, 0)$ for any τ , we obtain

$$\begin{aligned} x(t) &= \Phi(t, 0) \int_0^t \Phi^{-1}(\tau, 0) \mathbf{f}(\tau) d\tau \\ &= \Phi(t, 0) \left[\int_0^{nt_c} \Phi^{-1}(\tau, 0) \mathbf{f}(\tau) d\tau + \int_{nt_c}^t \Phi^{-1}(\tau, 0) \mathbf{f}(\tau) d\tau \right] \equiv \Phi(t, 0) [\mathbf{H}_1(n) + \mathbf{H}_2(t)]. \end{aligned} \quad (36)$$

The solution can be found in two distinct parts, namely for an integral number of mesh cycles (\mathbf{H}_1) and for the last cycle (\mathbf{H}_2). For n complete cycles, the expression for $\mathbf{H}_1(n)$ is found as

$$\mathbf{H}_1(n) = \sum_{i=1}^n \int_{(i-1)t_c}^{it_c} \Phi_i^{-1}(\tau, 0) \mathbf{f}(\tau) d\tau. \quad (37)$$

Now using Floquet theory [14], $\Phi_i^{-1}(\tau, 0) = [\Phi^{-1}(t_c, 0)]^{i-1} \Phi^{-1}(\tau, 0)$, we get

$$\begin{aligned}
 \mathbf{H}_1(n) &= \sum_{i=1}^n [\Phi^{-1}(t_c, 0)]^{i-1} \int_0^{t_c} \Phi_i^{-1}(\tau, 0) \mathbf{f}(\tau) d\tau \\
 &= \sum_{i=1}^n [\Phi^{-1}(t_c, 0)]^{i-1} \left[\begin{array}{l} \mathbf{W}_1(0) \int_0^{t_a} \mathbf{W}_1^{-1}(\tau) \mathbf{f}(\tau_0) d\tau \\ + \mathbf{W}_1(0) \mathbf{W}_1^{-1}(t_a) \mathbf{W}_2(t_a) \int_{t_a}^{t_b} \mathbf{W}_2^{-1}(\tau) \mathbf{f}(\tau_0) d\tau \\ + \mathbf{W}_1(0) \mathbf{W}_1^{-1}(t_a) \mathbf{W}_2(t_a) \mathbf{W}_2^{-1}(t_b) \mathbf{W}_3(t_b) \int_{t_b}^{t_c} \mathbf{W}_3^{-1}(\tau) \mathbf{f}(\tau_0) d\tau \end{array} \right],
 \end{aligned}
 \tag{38}$$

where $\tau_0 = \tau + (i - 1)t_c$. A similar approach is applied to the last time cycle, except that the value of $\mathbf{H}_2(t)$ will not depend upon the positioning of t in the whole mesh cycle and three possible solutions ensue:

$$\begin{aligned}
 \mathbf{H}_2(t) &= [\Phi^{-1}(t_c, 0)]^n \left[\mathbf{W}_1(0) \int_0^{t-nt_c} \mathbf{W}_1^{-1}(\tau) \mathbf{f}(\tau_0) d\tau \right], \quad 0 \leq t - nt_c < t_a, \\
 &= [\Phi^{-1}(t_c, 0)]^n \left[\begin{array}{l} \mathbf{W}_1(0) \int_0^{t_a} \mathbf{W}_1^{-1}(\tau) \mathbf{f}(\tau_0) d\tau \\ + \mathbf{W}_1(0) \mathbf{W}_1^{-1}(t_a) \mathbf{W}_2(t_a) \int_{t_a}^{t-nt_c} \mathbf{W}_2^{-1}(\tau) \mathbf{f}(\tau_0) d\tau \end{array} \right], \quad t_a \leq t - nt_c < t_b, \\
 &= [\Phi^{-1}(t_c, 0)]^n \left[\begin{array}{l} \mathbf{W}_1(0) \int_0^{t_a} \mathbf{W}_1^{-1}(\tau) \mathbf{f}(\tau_0) d\tau + \mathbf{W}_1(0) \mathbf{W}_1^{-1}(t_a) \\ \times \mathbf{W}_2(t_a) \int_{t_a}^{t_b} \mathbf{W}_2^{-1}(\tau) \mathbf{f}(\tau_0) d\tau + \mathbf{W}_1(0) \mathbf{W}_1^{-1}(t_a) \\ \times \mathbf{W}_2(t_a) \mathbf{W}_2^{-1}(t_b) \mathbf{W}_3(t_b) \int_{t_b}^{t-nt_c} \mathbf{W}_3^{-1}(\tau) \mathbf{f}(\tau_0) d\tau \end{array} \right], \quad t_b \leq t - nt_c.
 \end{aligned}
 \tag{39a-c}$$

In equation (39), $\tau_0 = \tau + nt_c$. If the period of the forcing function is the same as the parametric variation (t_c), such as in the case of gear meshing, then the integrals may be further simplified and all $f(\tau_0) \equiv f(\tau)$. For an equation with rectangular coefficients, the inverse of the transition matrix in equation (31) is found to be

$$\mathbf{W}^{-1}(t) = \frac{1}{\lambda_1 - \lambda_2} \begin{bmatrix} \lambda_2 e^{-\lambda_1 t} & -e^{-\lambda_1 t} \\ -\lambda_1 e^{-\lambda_2 t} & e^{-\lambda_2 t} \end{bmatrix}.
 \tag{40}$$

The various excitations are generically represented by equation (41), where i represents each continuous interval, and R_e and k_e are the equivalent base radius and stiffness parameters respectively.

$$\text{Mean torque: } f(\tau) \approx T_0.
 \tag{41a}$$

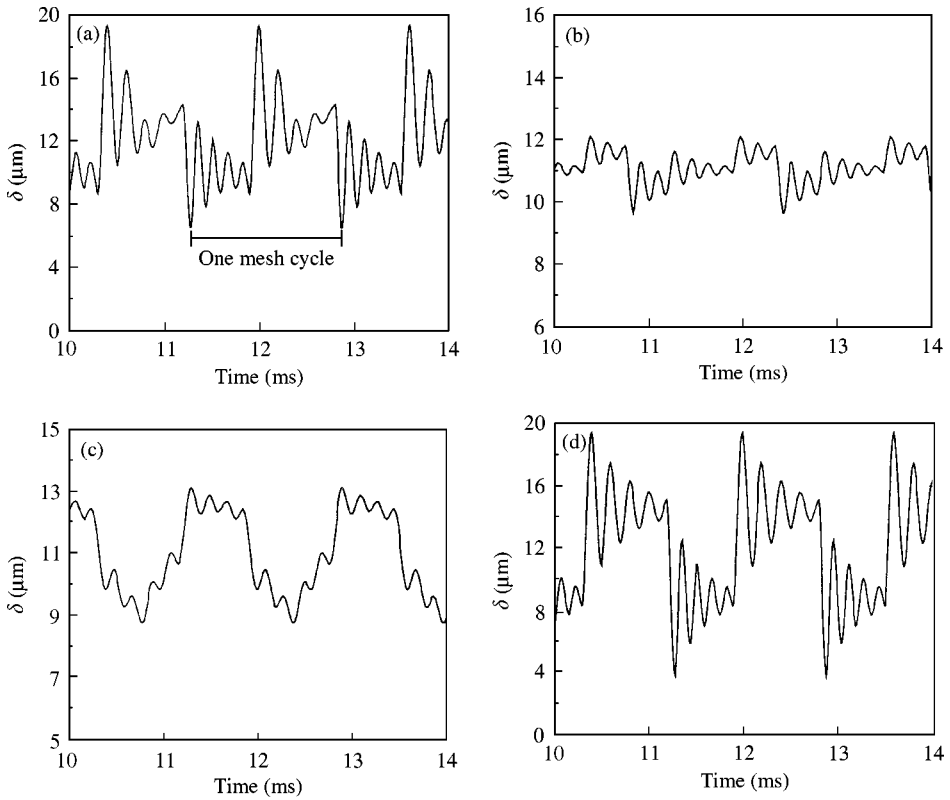


Figure 3. Dynamic transmission error due to individual and combined excitations. (a) All excitations combined; (b) only friction excitation $T_f(t)$; (c) only profile deviation $\varepsilon(t)$; (d) only parametric variations $k(t)$ and $c(t)$.

$$\text{Transmission error: } f(\tau) \approx k_e R_e \sum_i \varepsilon_i \cos(i\Omega\tau + \phi_i). \quad (41b)$$

$$\text{Friction torque: } f_1(\tau) \approx \beta_{1,i} + \beta_{2,i}\tau. \quad (41c)$$

5.3. TYPICAL RESULTS

For all of the excitations in equation (41), the integrals $\mathbf{H}_1(n)$ and $\mathbf{H}_2(t)$ are solvable in their closed form. With substitution in equations (38) and (39), the time-domain response of the gear system is calculated. Figure 3 shows the relative contribution of parametric stiffness and viscous damping variation, friction and profile deviations in terms of dynamic transmission error. A damping ratio of 5% is used and the value of friction coefficient μ_0 is taken as 0.1, both of which are representative of typical gear meshes under normal operating conditions. For non-parametric excitation results, the time-varying stiffness and viscous damping have been replaced by their time-averaged components, integrated over one full tooth mesh cycle. The frequency spectra for the same are shown in Figure 4. Note that since the analytical method does not stipulate any approximations in the process of solving equations, it precludes any potential errors. A comparison of $\delta(t)$ predicted by Floquet theory with results from numerical simulation showed the two to be identical, and

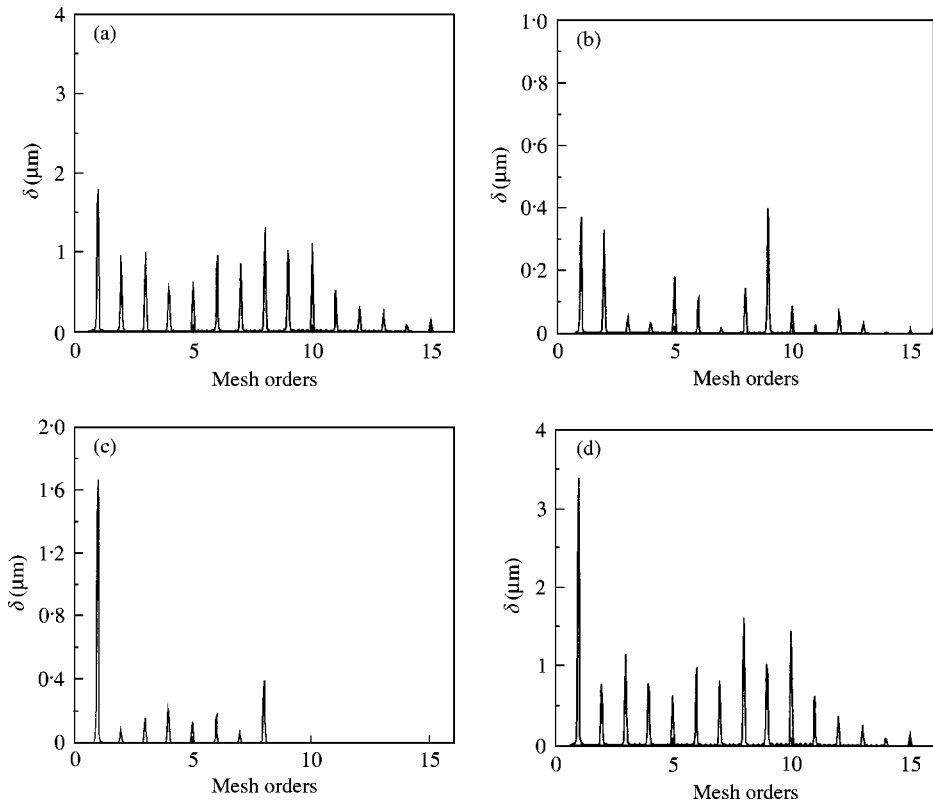


Figure 4. Spectral contents of DTE due to individual and combined excitations, corresponding to Figure 3. Only orders of the mesh harmonics exist. (a) All excitations combined; (b) only friction excitation $T_f(t)$; (c) only profile deviation $\varepsilon(t)$; (d) only parametric variations $k(t)$ and $c(t)$.

hence that comparison is not presented here. Nevertheless, this confirms the validity of our closed form solutions.

In all the time plots, the tooth cycle is clearly visible [shown explicitly in Figure 3(a)] as the fundamental meshing frequency. The smaller oscillations indicate the mean natural frequency of the torsional system, which is based on the time-averaged mesh stiffness, and it is found to be close to the ninth mesh harmonic. The two distinct regions can be seen in Figure 3(d) corresponding to single- and double-tooth contact. Conversely, there are three such regions in the friction plot [Figure 3(b)], and the reversal at pitch point can be seen during each mesh cycle. For both the cases, a strong superharmonic response can be observed in the frequency spectra [Figure 4(b, d)]. Both time traces and frequency spectra indicate that parametric variations have a rather dominant effect on the system response. Note that the total response in Figure 4(a) is smaller than that due to parametric variation alone in Figure 4(d), because the profile modifications are usually added in order to overcome some effects of the mesh stiffness variation. Friction force has a somewhat limited influence on torsional dynamics, except at higher harmonics of the meshing frequency. This situation can change at higher torque values, since friction increases in direct proportion to the mean applied torque. Thus, Floquet theory has been successfully applied to isolate and predict the dynamic behavior of the system under mixed excitation conditions. Our method presents a significant improvement over the solution strategy used by Hochmann [12], since we eliminate the Fourier series expansions and include parametric variations of

stiffness and sliding friction. The benefits of an analytical solution for the dynamic transmission error are even more apparent when aperiodic behavior over large intervals or instability characteristics are under investigation, as shown in the following sections.

6. STABILITY CONSIDERATIONS IN GEAR MESHES

6.1. FUNDAMENTAL CRITERIA FOR STABILITY

Asymptotic stability of a homogenous system can be determined from the discrete transition matrix over one complete period of parametric changes. Richards [15] has shown that a sufficient condition for stability is that all the eigenvalues of the state transition matrix have an absolute value less than unity, or $|\lambda_i| < 1 \forall i$. This principle is applied to predict instability for both formulations A and B, with the maximum absolute value of eigenvalues substituted in the above inequality. The discrete transition matrix, and consequently the stability, will be affected by many parameters, including rotational speed Ω_p , contact ratio Γ , coefficient of friction μ and viscous damping ratio ζ in the system. Figure 5 shows the mapping of the maxima of $|\lambda_i|$ for formulation B (which includes the friction term in the homogenous equation), as a function of rotational speed Ω_p and contact ratio Γ . In the absence of viscous damping, regions of asymptotic instability are distinctly identifiable as diagonally laid zones on the $\lambda(\Gamma, \Omega_p)$ map. As the contact ratio is incremented, the mean stiffness k_{mean} of the system goes up, and consequently the subharmonic frequencies increase. The presence of subharmonic resonances can also be seen in the spacing of unstable zones on the Ω_p axis, where for instance the zone containing 1500 rpm and $\Gamma = 1.24$ corresponds to the (2/17)th harmonic of the mean natural frequency, the zone immediately to its left corresponds to the one-ninth harmonic and so on.

6.2. DYNAMIC RESPONSE AND STABILITY RESULTS

To confirm the instability predictions in the system, the dynamic response of gears is found by applying a combined friction and parametric excitation. Figure 6 depicts the time

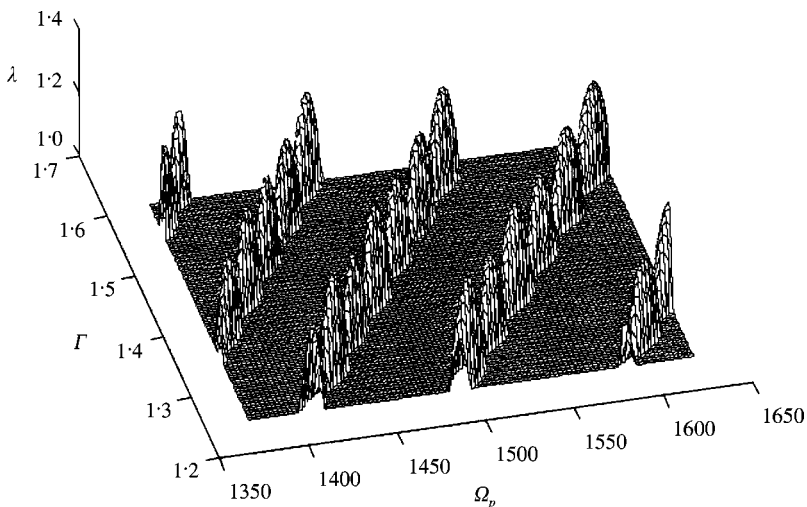


Figure 5. Stability parameter λ as a function of rotation speed Ω_p and profile contact ratio Γ , for a viscously undamped system.

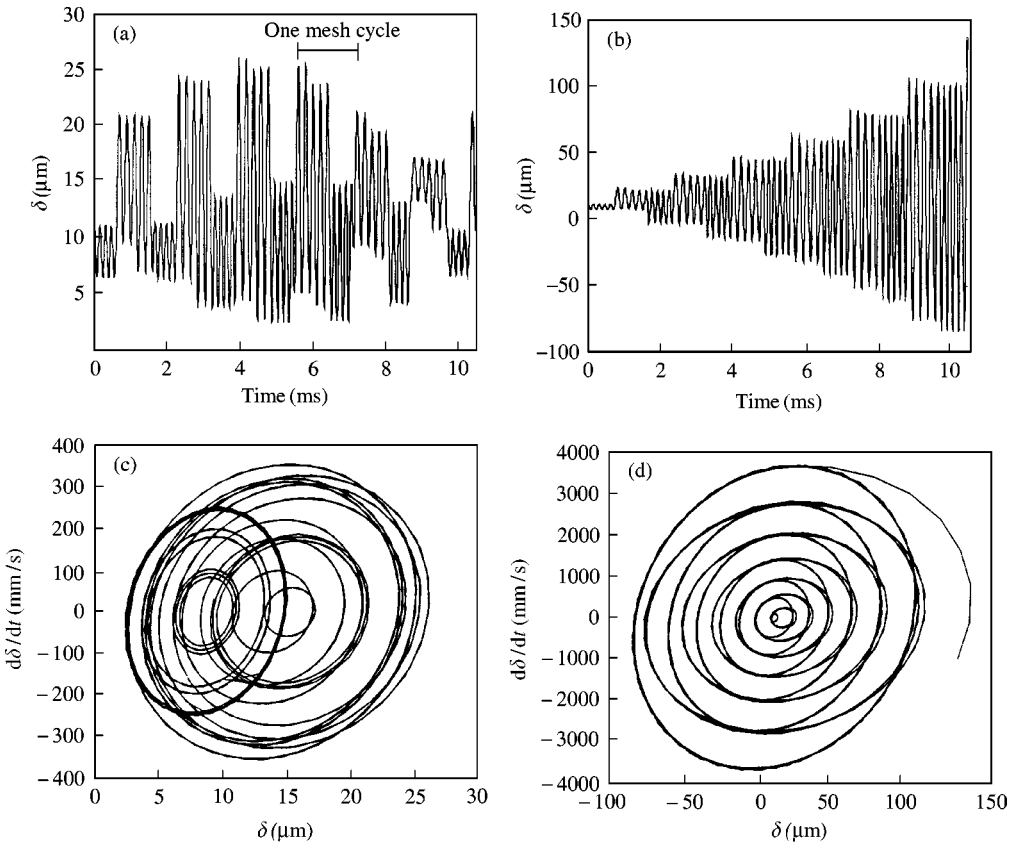


Figure 6. Dynamic transmission error for stable and unstable regions for $\varepsilon(t) = 0$, $\mu = 0.1$. (a) Time trace for stable region, $\Gamma = 1.374$, $\Omega_p = 1484$ rpm; (b) time trace for unstable region, $\Gamma = 1.453$, $\Omega_p = 1484$ rpm; (c) phase plane plot corresponding to (a); (d) phase plane plot corresponding to (b).

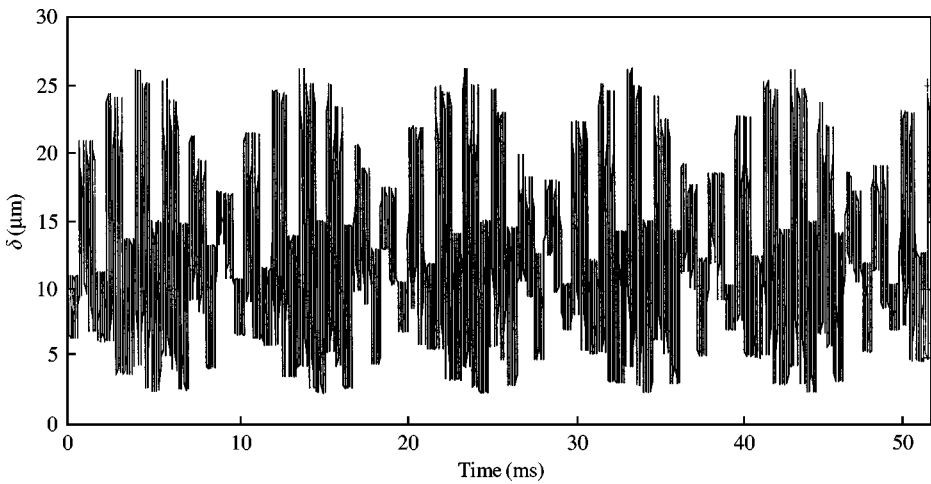


Figure 7. Long term stability of the system corresponding to Figure 6(a).

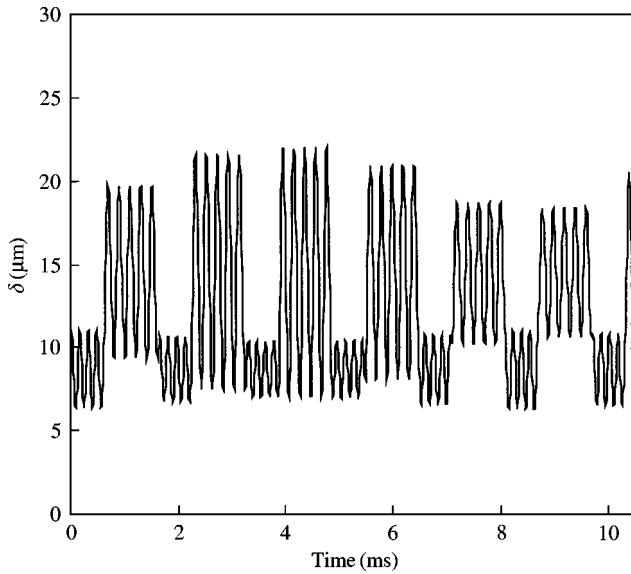


Figure 8. Response of the system corresponding to Figure 6(a), when $\mu = 0$ is chosen.

trace and the phase plane plots for the dynamic transmission error, when formulation B is applied, with no viscous damping in the system. It is evident that when parameters corresponding to an unstable case are used, the solution is unbounded as the elapsed time increases [Figure 6(b)]. The asymptotic instability is also apparent from the divergence observed in the phase plane plots [Figure 6(d)]. Similar to Figure 3, the mesh period and the mean natural frequency can be seen in Figure 6(a). Here, the change in the peak heights is caused by the frictional torque variation. In Figure 7, the extended time response is plotted, which shows that the system exhibits long-term stability and a periodic behavior. However, when the friction is removed, the peak-to-peak value of dynamic transmission error is reduced from 23 to 15 μm (Figure 8). A comparison with Figure 6(a) shows that in addition to amplifying the response, friction may also induce a significant modulation phenomenon.

6.3. INFLUENCE OF VISCOUS DAMPING AND SLIDING FRICTION

Next, the influence of sliding friction is examined on the stability contours, by comparing formulations A and B. Figure 9 shows the enlarged view of one particular instability region in terms of a Γ - Ω_p map, when no viscous damping is considered. Inclusion of friction has the effect of shifting this region a little towards the higher speed side. However, the overall influence is negligible, as confirmed by Figure 10, where the stability lines show a very weak dependence on μ . When the sliding friction is considered in the homogenous equation, it has primarily a mass-loading effect, and the exact shape of frictional torque variation does not appear to significantly affect the stability characteristics. This observation is valid only when the sliding friction is modelled using the LTV model. When sliding non-linearities are incorporated, friction could play a much larger role in stabilizing the system, since it is possible to obtain an equivalent damping coefficient for friction, by equating the energy loss due to two mechanisms.

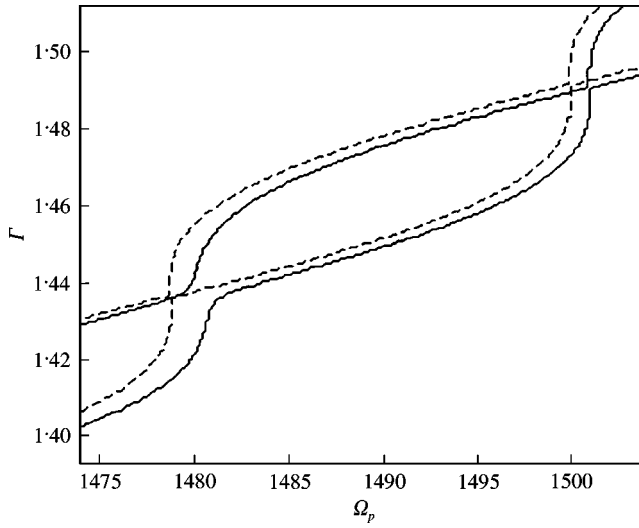


Figure 9. Effect of Coulomb friction on instability zone. Key: —, with friction; ---, without friction. Here the area enclosed within the curves is the unstable zone.

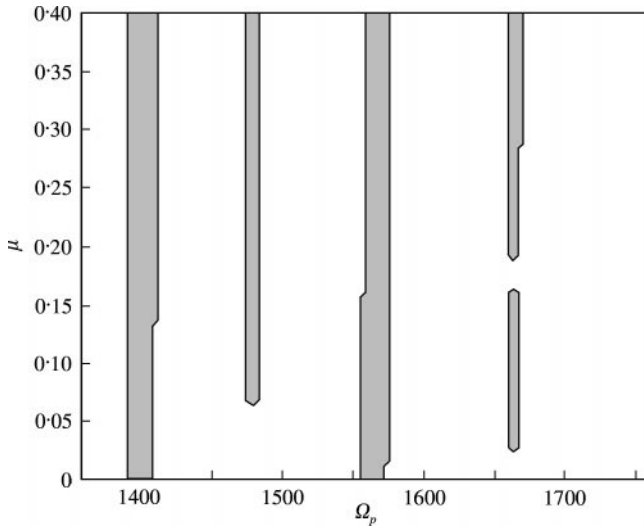


Figure 10. Stability contours for μ and Ω_p (rpm) when computed with formulation B. Here, shaded portions imply unstable zones.

Finally, the viscous damping term is included in the governing equations (Figure 11) and plotted against the profile contact ratio. It is apparent from the graph that for normal operating conditions of the gears, a viscous damping ratio value $\zeta > 0.01$ will always yield a stable solution. This is demonstrated by modifying the originally unstable system [Figure 6(b)], by adding a damping ratio value ζ of 0.01. Figure 12 shows that even though a large amplitude results, the response is asymptotically stable.

From this analysis, it can be deduced that under normal running conditions, the gear pairs pass through potential instability zones, which may result in a large dynamic factor

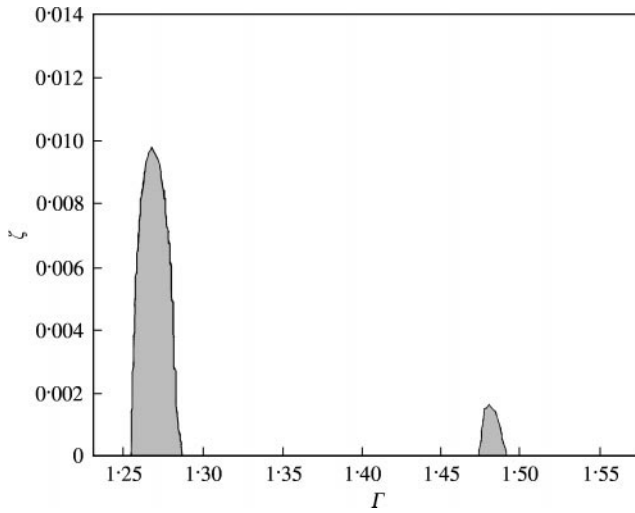


Figure 11. Stability boundary for contact ratio Γ and damping ratio ζ at $\Omega_p = 1500$ rpm, when computed with formulation A.

and vibro-acoustic response. These zones are sensitive to various design parameters, the most notable of which is the contact ratio of the gear mesh. On the other hand, although sliding friction as an LTV parameter alters the nature of the equations and solution methodology, it has only a marginal effect on the overall dynamic stability of the system. Besides, most practical gears will have sufficient viscous damping to prevent the occurrence of instabilities. Furthermore, backlash [9] as well as sliding non-linearities [14] could in fact result in stabilizing the system, especially at higher superharmonics. Nevertheless, sliding friction affects the spectral modulation characteristics and the forced response at higher torque loads.

7. CONCLUSION

In this paper, a new model and closed form solutions are developed that are expected to enhance our analyzing capability and the understanding of gear vibration and noise sources. A spur gear pair operating under Coulomb friction has been modelled as a linear time-varying system and it is shown that the manner in which friction is incorporated dictates the form of the governing differential equations. Our work overcomes the limitations of all known prior research work [3, 4, 10] that assumed friction to be a pure external excitation. Conversely, in this study, μ is shown to also affect the homogenous part of the equation, and thus it is treated as a system parameter. New analytical formulations are derived and verified for the two modelling scenarios in terms of exponential and Bessel functions, respectively, with the application of Floquet theory. Deficiencies of previous methods [12] are overcome by including periodic mesh stiffness and damping, and their dynamic interactions with sliding friction characteristics are studied. It is shown that profile deviations, friction and stiffness fluctuations, all generate a dynamic transmission error of a similar magnitude, with different spectral contents. Although it is the smallest contributor to peak transmission error, friction can yet have a large modulation effect on the response. Finally, classical stability theorems are applied by including sliding resistance, and it is

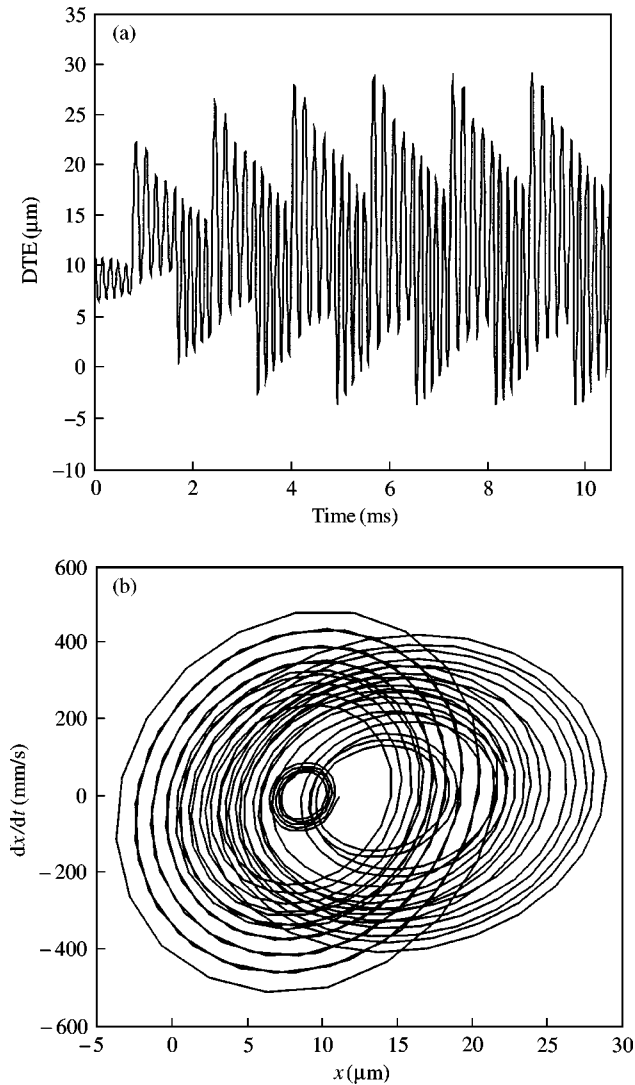


Figure 12. System response after inclusion of viscous damping with $\zeta = 0.01$: (a) time response; (b) phase plane plot.

observed that friction had only a minimal effect on the torsional instabilities of the gear dynamic system.

It is conceivable that a higher degree of freedom system, which includes flexural vibrations in the friction force direction (η), may show a much larger influence of sliding friction on the overall system behavior. Furthermore, when friction polarity is considered to be a function of the instantaneous surface velocity, rather than a quasi-static time-varying function, the sliding force modes may play a crucial role in the stability characteristics of the system. This will, of course, lead to non-linear model, which cannot be analyzed by the formulation of this article. Further research is under way to investigate this phenomenon. Similarly, one may include clearance non-linearities [9] and alternate cyclic variations of stiffness and examine the subsequent interactions.

ACKNOWLEDGMENT

The first author acknowledges the financial support from the Gear Dynamics and Gear Noise Research Laboratory, an industrial consortium at The Ohio State University.

REFERENCES

1. H. N. OZGUVEN and D. R. HOUSER 1988 *Journal of Sound and Vibration* **121**, 383–411. Mathematical models used in gear dynamics—a review.
2. J. BORNER and D. R. HOUSER 1996 *Technical Paper Series* 961816, *Society of Automotive Engineers*, 1–8. Friction and bending moments as gear noise excitations.
3. H. IIDA, A. TAMURA and Y. YAMADA 1985 *Bulletin of the Japanese Society of Mechanical Engineers* **28**, 1512–1519. Vibrational characteristics of friction between gear teeth.
4. E. RADZIMOVSKY and A. MIRAREFI 1974 *Journal of Engineering for Industry, Transactions of the American Society of Mechanical Engineers Paper no. 74-DET-86*, 1–7. Dynamic behavior of gear systems and variation of coefficient of friction and efficiency during the engagement cycle.
5. A. KAHRAMAN and R. SINGH 1990 *Journal of Sound and Vibration* **142**, 49–75. Non-linear dynamics of a spur gear pair.
6. C. PADMANABHAN and R. SINGH 1996 *Journal of Acoustical Society of America* **99**, 324–334. Analysis of periodically forced nonlinear Hill's oscillator with application to a geared system.
7. H. N. OZGUVEN 1991 *Journal of Sound and Vibration* **145**, 239–260. A non-linear mathematical model for dynamic analysis of spur gears including shaft and bearing dynamics.
8. T. IWATSUBO, S. ARII and R. KAWAI 1984 *Proceedings of the Third International Conference on Vibrations in Rotating Machinery, Institution of Mechanical Engineers*, 59–66. The coupled lateral torsional vibration of a geared rotor system.
9. A. KAHRAMAN and R. SINGH 1991 *Journal of Sound and Vibration* **146**, 135–156. Interactions between time-varying mesh stiffness and clearance non-linearities in a geared system.
10. S. OH, K. GROSH and J. R. BARBER 1998 *Proceedings of the National Conference on Noise Control Engineering, Ypsilanti, Michigan, USA, Institute of Noise Control Engineering*, 145–150. Dynamic behavior of interacting spur gears: energy conservation.
11. G. W. BLANKENSHIP and R. SINGH 1995 *Journal of Sound and Vibration* **179**, 13–36. Analytical solution for modulation sidebands associated with a class of mechanical oscillators.
12. D. HOCHMANN 1997 *Ph.D. Dissertation, The Ohio State University, Columbus, OH*. Friction force excitations in spur and helical involute parallel axis gearing.
13. A. S. KUMAR, T. S. SANKAR and M. O. M. OSMAN 1984 *Journal of Mechanisms, Transmissions and Automation in Design, Transactions of the American Society of Mechanical Engineers Paper no. 84-DET-212*, 1–7. On dynamic tooth load and stability of a spur-gear system using the state-space approach.
14. M. BENTON and A. SEIREG 1978 *Journal of Mechanical Design, Transactions of the American Society of Mechanical Engineers* **100**, 26–32. Simulation of resonances and instability conditions in pinion-gear systems.
15. J. A. RICHARDS 1983 *Analysis of Periodically Time-Varying Systems*. New York: Springer.
16. V. V. BOLOTIN 1964 *Dynamic Stability of Elastic Systems*. San Francisco: Holden-Day, Inc.
17. E. A. BARBASHIN 1970 *Introduction to the Theory of Stability*. Netherlands: Wolters-Noordhoff.

APPENDIX A: NOMENCLATURE

c	viscous damping coefficient
F	force
\mathbf{f}	generalized force vector
\mathbf{G}	system matrix
J	moment of inertia
k	mesh stiffness
m	mass for a translational system
N	normal load function
n	integral number of mesh cycles
R	base circle radius

T	torque
t	time instant
\mathbf{W}	Wronskian matrix
\mathbf{x}	generalized displacement vector
α	gear roll angle
β, γ	generalized parameters
δ	dynamic transmission error
ε	unloaded static transmission error
Φ	state transition matrix
φ	pressure angle of the gears
Γ	profile contact ratio of gears
η	axis along off-line of action
λ	eigenvalue of state transition matrix
μ_0	coefficient of friction of the gear material
μ_i	instantaneous coefficient of friction for i th tooth
Π	number of teeth on gear or pinion
θ	angle of rotation of gear or pinion
τ	cyclic time variable
Ω	mean angular speed
ξ	axis along the line of contact
ζ	viscous damping ratio

Subscripts

1, 2	number of tooth in contact
a, b, c	time zone in gear mesh cycle
e	equivalent system
f	sliding friction
m	one mesh cycle
p, g	pinion and gear respectively